

Nonuniform Charge Effects in Protein–Protein Interactions

M. L. Grant*

Department of Chemical Engineering, Yale University, P.O. Box 208286, New Haven, Connecticut 06520-8286

Received: October 27, 2000; In Final Form: February 2, 2001

Two phenomena reduce the electrostatic repulsion between protein molecules in solution: charge heterogeneity (patchiness) and charge fluctuation. In this work, the electrostatic interaction energy for two protein molecules is computed as a function of separation and orientation. The results are based on solutions of the linearized Poisson–Boltzmann equation for an arbitrary prescribed surface charge distribution. A boundary element technique yields a numerical solution for the electrostatic potential on the protein surface that is then used to compute the reversible charging work. The results indicate that the two mechanisms act in a complementary fashion. Correlations in charge fluctuations reduce the net charge on the molecules and produce a long-range effect, while charge patchiness becomes significant at separations smaller than the Debye length. Both effects are included in a DLVO-type interaction potential that is used to match published second virial coefficients of lysozyme. Compared to earlier studies, the best-fit values of the effective Hamaker constant are much less sensitive to ionic strength and in better agreement with estimates based on Lifshitz theory.

Introduction

The thermodynamic behavior of protein solutions is determined by protein–protein interactions. For dilute solutions of protein, it is sufficient to focus on interactions involving only two protein molecules. Electrostatic interactions are of primary importance because proteins tend to be highly charged and protein solutions have relatively high ionic strengths (10 mM and higher). Most treatments of protein–protein electrostatics employ the linearized Poisson–Boltzmann (Debye–Hückel) equation with various descriptions of the protein's charge distribution.^{1–7} The simplest models treat the protein as uniformly charged spheres, while others include some higher-order multipoles to handle the effects of the nonuniform charge distribution on the protein surface. When the charge distribution is nonuniform, the proteins favor low-energy orientations, and the effective repulsion between molecules is less than that for equivalent uniform molecules.

Kirkwood and Shumaker¹ and Phillies⁸ employed a multipole expansion to study the effects of charge fluctuation on protein–protein electrostatics. They looked at terms through the dipole–dipole interaction but focused on the asymptotic behavior of the interaction potential under isoionic conditions where the net charge on the protein is zero. The charge fluctuations on the two molecules are independent at infinite separation but become correlated as the molecules approach. Again, the molecules tend to favor low-energy charge states, and the repulsion is reduced relative to proteins with fixed charges.

Numerical methods have been developed to solve the linearized Poisson–Boltzmann equation for arbitrary charge distributions and geometries,^{9–11} so the combined effects of charge heterogeneity and charge fluctuation can be quantified. Moreover, numerical methods such as the boundary element method used in this study account for all multipoles in the protein charge distribution and provide solutions even at contact, when multipole expansions normally do not converge.^{12,13}

In this paper, the effects of these phenomena are quantified through sample calculations for hen egg white lysozyme, a globular protein that has an approximate molecular weight of 14 000 and a hydrodynamic radius of 20 Å. The presentation begins with a description of the boundary element method used to solve the electrostatics equations. The solutions are then used to compute the electrostatic interaction energy between two molecules, with various models for the charge distribution. Finally, the results are used to fit experimental measurements of the second virial coefficient of hen lysozyme solutions. Both phenomena are shown to make important contributions to the virial coefficients at small separations.

Method

A boundary element method is used to calculate the electrostatic potential on the surface of the molecules by solving Laplace's equation inside the protein molecules (region 1) and the Debye–Hückel equation in the electrolyte solution (region 2)

$$\text{inside: } \nabla^2 \psi_1 = 0 \quad (1)$$

$$\text{outside: } \nabla^2 \psi_2 = \kappa^2 \psi_2$$

where ψ is the electrostatic potential and $\kappa = [(2000N_A e^2 / \epsilon_0 \epsilon_2 kT)I]^{1/2}$; N_A is Avogadro's number, e is the elementary charge, ϵ_0 is the permittivity of free space, ϵ_2 is the dielectric constant of the solution ($\epsilon_2 = 80$), k is Boltzmann's constant, T is the absolute temperature, and I is the ionic strength of the solution in mol/liter. At the surface of the molecules, the boundary conditions are the continuity of potential and the jump in electric displacement

$$\psi_1 = \psi_2 \quad (2)$$

$$\epsilon_1 \nabla \psi_1 \cdot \mathbf{n} - \epsilon_2 \nabla \psi_2 \cdot \mathbf{n} = \sigma / \epsilon_0 \quad (3)$$

where σ is the fixed surface charge density, $\epsilon_1 = 2$, and \mathbf{n} is the unit normal directed away from the molecule.

* Phone: (203) 432-4376. Fax: (203) 432-4387. Email: marshall.grant@yale.edu.

The electrostatic contribution to the interaction potential is given by^{14–16}

$$\Phi_{\text{elec}}(r) = \frac{1}{2} \frac{\int \sigma \psi(r) dA}{A_1 + A_2} - \frac{1}{2} \frac{\int \sigma \psi_{\infty} dA}{A_1 + A_2} \quad (4)$$

where $W(r)$ is the reversible charging work required to assemble the fixed surface charges on the proteins when their center–center separation is r and W_{∞} is the charging work when the molecules are infinitely separated. The integration is performed over the surfaces of both particles ($A_1 + A_2$). For uniform spheres, $\psi_{\infty} = \sigma a / [\epsilon_0 \epsilon_2 (1 + \kappa a)]$, and the self-energy of a single molecule is proportional to the square of the net valence on the molecule, $W_{\text{self}} = Z^2 e^2 / [8\pi \epsilon_0 \epsilon_2 a (1 + \kappa a)]$; $W_{\infty} = 2W_{\text{self}}$.

The protein molecules are treated as spheres with a specified surface charge distribution. The molecule boundary is defined as the best-fit sphere that comes closest to the crystallographically determined coordinates of the charged groups on the molecule.¹¹ For lysozyme, the best-fit radius is $a = 16.5$ Å. The surface of each molecule is discretized into $N_1 = N_2 = 120$ spherical triangular elements, each having a uniform surface charge density, normal flux, and surface potential. Strictly, the properties obtained from a boundary element solution are associated with specific points or “nodes” on the surface,¹⁷ but in this “constant element” approximation, the nodes are located in the center of the elements, and the distinction is immaterial. Here, the surface charge density on each element, σ_i , is known, and the corresponding surface potential ψ_i is obtained from the boundary element solution of eqs 1–3. With the constant-element assumption, the integrals in eq 4 can be approximated by sums to obtain

$$\Phi_{\text{elec}}(r) \approx \frac{1}{2} \sum_{i=1}^{N_1+N_2} \sigma_i \psi_i(r) A_i - \frac{1}{2} \sum_{i=1}^{N_1+N_2} \sigma_i \psi_{i,\infty} A_i \quad (5)$$

where A_i is the area of element i . (In these calculations, the A_i values are identical.)

Four different models for the surface charge distribution were employed: fixed uniform, fixed heterogeneous, fluctuating uniform, and fluctuating heterogeneous.

The simplest approach is to treat the proteins as uniformly charged particles with a net charge calculated from the protein’s amino acid sequence and the pK_a of the ionizable groups (taken to be the same as small-molecule analogues¹⁸) under the assumption that the acid–base equilibria are independent. The average charge of an acid group, which can be neutral or negative, is assumed to be $z_{\text{acid}} = -p_-$, where $p_- = K_a / (K_a + [H^+])$ is the fractional dissociation of that acid group.¹ Similarly, the average charge on a basic group is $z_{\text{base}} = p_+ = [H^+] / (K_a + [H^+])$, where p_+ is the fractional protonation of the group. The net charge on the molecule is

$$\bar{Z} = \sum_{\text{bases}} p_+ - \sum_{\text{acids}} p_- \quad (6)$$

and the uniform surface charge density is $\sigma = \bar{Z}e / 4\pi a^2$.

Rather than treat the molecule as uniform, the second model accounts for the nonuniform arrangement of charge on the protein surface by representing each charge as a 100 Å² spherical cap centered on the location of the ionizable group. The interaction potential in this case depends on the orientation of

the molecules, Ω , and the effective angle-averaged interaction potential is

$$\Phi_{\text{elec}}(r) = \langle W(r) \rangle - W_{\infty} \quad (7)$$

where^{15,19}

$$\langle W(r) \rangle = -kT \ln \left\{ \frac{\int \exp[-W(r, \Omega)/kT] d\Omega}{\int d\Omega} \right\} \quad (8)$$

In this case, ψ_{∞} varies with location on the surface, but W_{∞} , which is independent of orientation, is still computed as in eq 4. At each separation, orientations are sampled as follows: First, the spheres are oriented so that node i on sphere 1 directly faces node j on sphere 2. Sphere 2 is then rotated about the line of centers in 120° increments to obtain two more orientations. By repeating this process for all possible pairs of opposing nodes, we sampled a total of $N_{\Omega} = N_1 \times N_2 \times 3 = 120 \times 120 \times 3 = 43\,200$ orientations are sampled. Not all of these orientations are unique since an ij interaction is equivalent to a ji interaction. $\langle W(r) \rangle$ is then approximated by

$$\langle W(r) \rangle \approx -kT \ln \left\{ \frac{1}{N_{\Omega}} \sum_{\text{orientations}} \exp[-W(r, \Omega)/kT] \right\} \quad (9)$$

The charge assignment procedure described above represents an “average” molecule and is most appropriate when the pH is far from the pK_a s of the ionizable groups, i.e., when the titration curve is nearly flat. Lysozyme, however, is typically crystallized at pH 4–4.6, which is close to the pK_a of most carboxylic acids. At this pH, the acid groups are nearly equally distributed between their charged and neutral states, and the average charge may not be the most appropriate representation. The parameters p_+ and p_- , which are treated as the fractional charges in the first two models, can also be interpreted as the probability that a given group is charged. Under the assumption of independent acid–base equilibria, the probability distribution function (pdf) for the protein’s net charge $f_0(Z)$ can be calculated by enumerating the possible charge states for the ionizable groups, weighting each by the product of the associated probabilities, and summing all the weights corresponding to a given net charge. The effective interaction potential is then calculated from $\Phi_{\text{elec}}(r) = \langle W(r) \rangle - \langle W_{\infty} \rangle$ where

$$\langle W(r) \rangle = -kT \ln \left\{ \sum_{Z_1} \sum_{Z_2} f_0(Z_1) f_0(Z_2) \exp[-W(r, Z_1, Z_2)/kT] \right\} \quad (10)$$

$$\langle W_{\infty} \rangle = 2\langle W_{\text{self}} \rangle = -2kT \ln \left\{ \sum_{Z_1} f_0(Z_1) \exp[-W_{\text{self}}(Z_1)/kT] \right\} \quad (11)$$

Note that the average fixed charge used in the first model is recovered by setting $\bar{Z} = \sum Z f_0(Z)$.

In the final model, charge fluctuation and charge heterogeneity are combined. Because the interaction energy depends on both the net charge and the location of those charges, the effective interaction potential must be calculated from the charging work averaged over all orientations, Ω , and charge states, \mathbf{q}

$$\langle W(r) \rangle \approx -kT \ln \left\{ \frac{1}{N_{\Omega}} \sum_{\text{orientations}} \sum_{\mathbf{q}_1} \sum_{\mathbf{q}_2} f(\mathbf{q}_1) f(\mathbf{q}_2) \exp[-W(r, \Omega, \mathbf{q}_1, \mathbf{q}_2)/kT] \right\} \quad (12)$$

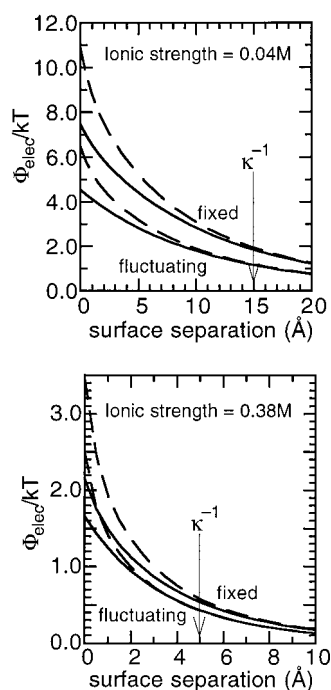


Figure 1. Electrostatic interaction potential, Φ_{elec} , for the four charge distribution models. Dashed curves represent uniform surface charge densities while the solid curves represent “patchy” charge distributions. The upper two curves are the results for static charge distributions, and the lower two curves describe the interaction energy for proteins with fluctuating charges.

where the vector \mathbf{q} is an ordered list representing the charge state of all the ionizable groups on the protein and $f(\mathbf{q})$ is the probability the protein is in that particular charge state. The probability is computed in a procedure analogous to that used to compute $f_0(Z)$ in the previous model. While it is straightforward to construct the pdf for the uniformly charged protein model with N charged groups ($N \geq 30$), it is impractical to fully sample all of a protein’s 2^N unique charge states. It is important, however, to sample enough states to estimate the interaction energy reliably. A method for selecting a subset of charge states is described next.

The tendency of each ionizable group to exist in both charged and uncharged forms is quantified by its variance, $s^2 = p(1 - p)$, which is a maximum of 0.25 at the pK_a (where $p = 1 - p = 0.5$) and decreases rapidly away from the pK_a . The variance for each of protein’s ionizable groups is calculated and ranked in descending order. A list of possible charge states is generated by allowing a number, n_v , of the most variable groups to assume both charged and uncharged states while the rest of the ionizable groups are assigned their more probable state. Typically, $n_v = 10$, which produces 1024 charge states. Once the charge states have been enumerated, the self-energy for an isolated molecule is calculated for each charge state, and its contribution to the “partition function” of the molecule, $\bar{f}(\mathbf{q}) = f(\mathbf{q}) \exp[-W_{\text{self}}(\mathbf{q})/kT]$, is computed. The charge configurations are then ranked in descending order of $\bar{f}(\mathbf{q})$, and the interaction potential is computed for interactions in which each molecule assumes the 32 states with the largest values of \bar{f} . Neglecting the other charge states in the summations of eq 12 is equivalent to assuming that $W(r, \Omega, \mathbf{q}_1, \mathbf{q}_2)$ is infinite for the unsampled states and leads to an upper bound for $\langle W \rangle$.

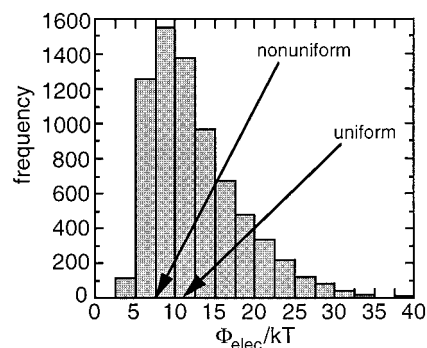


Figure 2. Histogram of Φ_{elec} at contact for two lysozyme molecules with fixed patchy charges at pH 4.3, 25 °C, and $I = 40$ mM. The value from the uniformly charged model is approximately 11 kT, while the Boltzmann-weighted angle average for the patchy model is 7.5 kT.

Results

Calculations were performed for hen egg white lysozyme at 25 °C, pH 4.3 (40 mM sodium acetate buffer), and ionic strengths of 40 mM (no added salt) and 0.38M (20 mg/mL added NaCl). The lysozyme molecule is approximated by a sphere of radius $a = 16.5$ Å. At pH 4.3, the net charge on lysozyme computed from eq 6 is $Z \approx 12$, based on 1 $\alpha\text{-NH}_3^+$ ($pK_a = 9.2$, $p_+ \approx 1$), 1 $\alpha\text{-COO}^-$ ($pK_a = 2.0$, $p_- = 0.99$), and the following side chain groups: 6 lysine ($pK_a = 10.8$, $p_+ \approx 1$), 11 arginines ($pK_a = 12.5$, $p_+ \approx 1$), 2 glutamic acids ($pK_a = 4.3$, $p_- = 0.5$), 1 histidine ($pK_a = 6.0$, $p_+ = 0.98$), 7 aspartic acids ($pK_a = 3.9$, $p_- = 0.72$), and 3 tyrosines ($pK_a = 10.9$, $p_- \approx 0$). Under these conditions, which are the same as those used by George and Wilson,²⁰ the interaction potential for uniformly charged particles at contact is approximately 11 kT ($I = 0.04$ M) and 3.4 kT ($I = 0.38$ M). The full electrostatic interaction potential curves calculated for each model are shown in Figure 1. Each form of heterogeneity reduces the effective repulsion between the proteins, and the effect is most pronounced at small particle–particle separations. The results for each of the other three electrostatic models are discussed below.

When two particles with fixed patchy charges interact, the interaction energy varies with orientation. This variability is well represented as a histogram of interaction energies, such as the one in Figure 2. Even though the histogram is skewed toward large repulsive energies, the Boltzmann weighting favors low-energy orientations and reduces the repulsion by about 30% compared with the corresponding uniform molecules. Since both models employ the same net charge, the curves for the two models are essentially the same at separations greater than about κ^{-1} . Higher-order multipoles have significantly shorter ranges than the monopole interactions and significantly reduce the repulsion between proteins at separations less than about κ^{-1} .

For proteins with fluctuating charges, the charging work for two proteins at separation r can be written as

$$\frac{W(r, Z_1, Z_2)}{kT} = \frac{W_{\text{self}}(Z_1)}{kT} + \frac{W_{\text{self}}(Z_2)}{kT} + Z_1 Z_2 \phi_1(r) + (Z_1^2 + Z_2^2) \phi_2(r) \quad (13)$$

where ϕ_1 accounts for charge–charge interactions between the molecules and ϕ_2 accounts for the influence of the low-dielectric interior of one protein on the charging work of the other; both ϕ_1 and ϕ_2 are nonnegative, and ϕ_2 is much shorter-ranged than ϕ_1 . An asymptotic expression for Φ_{elec} is obtained by expanding $\exp[-W(r, Z_1, Z_2)/kT]$ to second order in ϕ_i to give

$$\exp[-W(r, Z_1, Z_2)/kT] = e^{-W_{\text{self}}(Z_1)/kT} e^{-W_{\text{self}}(Z_2)/kT} \left\{ 1 - \right. \\ \left. Z_1 Z_2 \phi_1 - (Z_1^2 + Z_2^2) \phi_2 + \frac{1}{2} [Z_1^2 Z_2^2 \phi_1^2 + 2Z_1 Z_2 (Z_1^2 + Z_2^2) \phi_1 \phi_2 + (Z_1^2 + Z_2^2)^2 \phi_2^2] \right\} \quad (14)$$

and substituting into eq 10. The sum of self-energy terms can then be factored out to give

$$\langle W \rangle = -kT \ln \left\{ \underbrace{\sum_{Z_1} f_0(Z_1) e^{-W_{\text{self}}(Z_1)/kT} \sum_{Z_2} f_0(Z_2) e^{-W_{\text{self}}(Z_2)/kT}}_{\langle W \rangle_{\infty}} \right\} \\ - kT \ln \left[1 - \langle Z \rangle^2 \phi_1 - 2 \langle Z^2 \rangle \phi_2 + \frac{1}{2} (\langle Z^2 \rangle^2 \phi_1^2 + 2 \langle Z^3 \rangle \langle Z \rangle \phi_1 \phi_2 + (\langle Z^4 \rangle + \langle Z^2 \rangle^2) \phi_2^2] \right] \quad (15)$$

where

$$\langle Z^n \rangle = \frac{\sum_Z Z^n f_0(Z) e^{-W_{\text{self}}(Z)/kT}}{\sum_Z f_0(Z) e^{-W_{\text{self}}(Z)/kT}} \quad (16)$$

in agreement with Hill.¹⁴ Compared with the case of independent acid–base equilibria, correlation between ionizable groups reduces the average charge on the isolated protein from $\bar{Z} \approx 12$ to $\langle Z \rangle \approx 9.5$ at $I = 40$ mM and $\langle Z \rangle \approx 10.3$ at 0.38 M.

Since $\Phi = \langle W \rangle - \langle W \rangle_{\infty}$, the first term on the right-hand side of eq 15 cancels, and the asymptotic interaction potential is obtained by expanding the logarithm in the second term

$$\frac{\Phi_{\text{elec}}}{kT} = \langle Z \rangle^2 \phi_1 + 2 \langle Z^2 \rangle \phi_2 + \frac{1}{2} (\langle Z^4 \rangle - \langle Z^2 \rangle^2) \phi_1^2 + \\ 2 (\langle Z^2 \rangle \langle Z^2 \rangle - \langle Z^3 \rangle \langle Z \rangle) \phi_1 \phi_2 + (\langle Z^2 \rangle^2 - \langle Z^4 \rangle) \phi_2^2 \quad (17)$$

The linear terms in ϕ_i represent the interaction between proteins with charge $\langle Z \rangle$, while the second-order terms arise from charge fluctuations. At large separations, $\phi_2 \ll \phi_1 < 1$, and the repulsion is proportional to $\langle Z \rangle^2$, while the corresponding expression for independent equilibria and fixed uniform charges gives a repulsion proportional to $(\bar{Z})^2$. Thus, charge correlation reduces the asymptotic repulsion by 37% at $I = 40$ mM and by 26% at $I = 0.38$ M. The dominant charge-fluctuation term is attractive since $\langle Z^4 \rangle - \langle Z^2 \rangle^2 < 0$.^{8,14} At small separations, charge correlation effects are large. For lysozyme at pH 4.3, the repulsion between molecules at contact is reduced from 11 to 6.5 kT ($I = 0.04$ M) and from 3.5 to 2.5 kT ($I = 0.38$ M).

To complete the study, we include both charge heterogeneity and charge fluctuation in the final model. The correlation in acid–base equilibria again reduces the average charge on the protein and the asymptotic repulsion between molecules. At smaller separations, the charge heterogeneity permits orientation of the molecules to minimize repulsion. For lysozyme at pH 4.3, the relative reduction in the near-contact repulsion is about 35% compared with the fluctuating uniform charge model. Both types of charge variation lead to significant deviations of the interaction potential from that calculated for uniformly charged proteins.

In addition to ionic strength, pH also affects charge variability. Since the protein's charges arise from acid–base equilibrium, the location of the charges and the resulting multipole moments change with pH. Effects of charge patchiness are greatest at pHs where the charge distribution is most "lopsided." In contrast, charge correlation is most important at the pK_a of the carboxylic

acids (pH ~ 4 – 4.5) and again near pH ~ 10 – 11 when the basic groups are near their pK_a 's. Lysozyme's pI is ~ 11 , and calculations there reveal a weak long-range attraction and a short-range repulsion arising from the interaction between the charge on one molecule and the low-dielectric interior of the other; the interaction is described by ϕ_2 in eq 13. If the electrostatics alone determined the behavior of lysozyme, the molecules would eventually reside in shallow minima. Additional calculations for lysozyme near neutral pH show that charge fluctuation can be neglected.

The calculations indicate that spatial variation (charge patchiness) and temporal variation (charge fluctuation/correlation) both reduce the repulsion between proteins in solution. The primary effect of charge correlation is to lower the repulsion by reducing the average charge on the molecule. This mechanism is significant at all separations but is dominant at separations large compared with κ^{-1} . Patchiness produces an orientation-dependent distribution of energies, some of which are lower than that for equivalent uniform spheres. Molecular orientation effects are important at separations less than κ^{-1} , when the higher order multipoles of the charge distribution dominate the protein–protein interaction. In the next section, some consequences of these effects are investigated.

Application to Virial Coefficients in Dilute Lysozyme Solution. Statistical mechanics provide the connection between the thermodynamics of protein solutions and the underlying interaction potential $\Phi(r)$. For instance, analysis of osmotic pressure measurements on dilute protein solutions yields values for the second virial coefficient, B_2 , which is given by an integral of the interaction potential^{2,14,15}

$$B_2 = 2\pi \frac{N_A}{M} \int_0^{\infty} (1 - e^{-\Phi(r)/kT}) r^2 dr \quad (18)$$

where M is the molecular weight of the protein.

The behavior of protein systems has been successfully interpreted using colloidal interaction theory.^{3,4} In the standard Derjaguin–Landau–Verwey–Overbeek (DLVO) model of colloidal interactions, the form of the interaction potential is assumed to be

$$\Phi = \Phi_{\text{hs}} + \Phi_{\text{elec}} + \Phi_{\text{vdw}} \quad (19)$$

where Φ_{hs} is the excluded volume (hard sphere) contribution, Φ_{elec} is the electrostatic contribution given by the calculations described above, and Φ_{vdw} is the van der Waals attraction arising from induced dipole fluctuations.^{21–24} Additional phenomena such as hydrophobic interactions and hydrogen bonding are not included. In the Hamaker treatment, $\Phi_{\text{vdw}} = -A_{\text{eff}} f(r)$, where $f(r)$ is a dimensionless function of particle geometry and separation obtained by integrating the r^{-6} attraction over the volume of the interacting bodies; for two identical spheres of radius a ²³

$$\Phi_{\text{vdw}} = -A_{\text{eff}} f(r) = -A_{\text{eff}} \frac{1}{6} \left[\frac{2a^2}{r^2 - 4a^2} + \frac{2a^2}{r^2} + \ln \left(\frac{r^2 - 4a^2}{r^2} \right) \right] \quad (20)$$

Φ_{vdw} given by eq 20 diverges as $r \rightarrow 2a$, so the interaction is typically truncated at a surface–surface separation of $r - 2a = 1$ Å.

The uncertainties associated with each of the three terms in eq 19 are very different. Typically, the excluded volume contribution to B_2 is estimated accurately from the size of the protein inferred from hydrodynamic measurements or from low

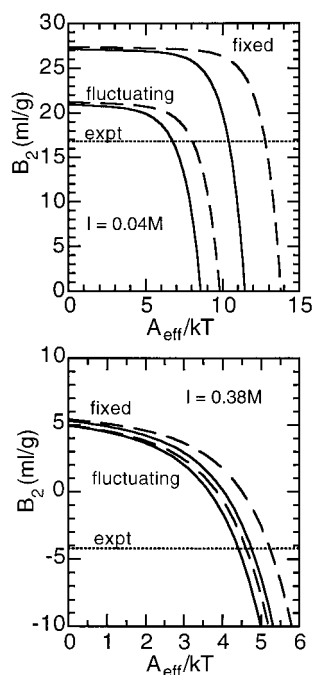


Figure 3. Second virial coefficient (B_2) for lysozyme as a function of the effective Hamaker constant for four charge distribution models. The experimental values are from George and Wilson.²⁰ The upper two curves are for fixed charge distributions and the lower two curves are for fluctuating charge distributions. Dashed curves, uniform surface charge density; solid curves, patchy charge distribution.

resolution X-ray diffraction. The electrostatics, as shown above, can be calculated to the accuracy of the chosen model. Φ_{vdw} , however, is so poorly known that it is usually estimated from fitting experimental data after the other terms have been determined. The van der Waals term must then compensate for any error introduced in the first two terms. Consequently, the apparent strength of the van der Waals attraction can be extremely sensitive to solution conditions such as ionic strength and pH.⁴ Such variation in A_{eff} , which is not consistent with the underlying theory, reduces the predictive value of the DLVO calculations. The results of the previous section suggest that a more detailed representation of the protein–protein electrostatics may reduce the apparent variability in A_{eff} and produce a more consistent description of protein–protein interactions in solution.

As an example, A_{eff} for lysozyme at pH 4.3 and 25 °C is determined by matching experimental measurements of B_2 .²⁰ For each of the four surface charge models discussed (fixed uniform, fixed patchy, variable uniform, and variable patchy), B_2 is calculated from eq 18, with A_{eff} as the only adjustable parameter (Figure 3). Φ_{vdw} is truncated at a 1 Å surface–surface separation in these calculations, i.e., $\Phi_{\text{vdw}} = \max[\Phi_{\text{vdw}}(2a+1 \text{ Å}), \Phi_{\text{vdw}}(r)]$. $A_{\text{eff}} \approx 13 \text{ kT}$ to balance the repulsion between identical uniform molecules at low ionic strength (40 mM) but only 5.4 kT at $I = 0.38 \text{ M}$. These values are comparable to others based on the “standard” DLVO assumption of uniform surface properties,^{3–5} but the large discrepancy between the two values indicates the shortcomings of the assumption. Both values, however, are significantly higher than the value of 3.1 kT calculated from Lifshitz theory by Roth, Neal, and Lenhoff.²⁵

When the “patchy sphere” model is used to describe the charge distribution, A_{eff} is reduced to approximately 10.4 kT at 40 mM and 4.8 kT at 0.38 M. When charge correlation is included, the dramatic reduction in protein–protein repulsion is reflected in the best-fit values of A_{eff} . For lysozyme with fluctuating uniform charges, the values of A_{eff} fall to 8.0 and

4.6 kT, while patchy fluctuating charges give 6.8 and 4.4 kT. These final values agree with each other within 55% while, the values obtained for the static uniform charge model differ by about 140%. Moreover, the final values are in much better agreement with Roth’s estimate from Lifshitz theory.

Several additional factors suggest that the values of A_{eff} obtained here are upper bounds. First, the boundary element calculations are performed with only 120 elements on each molecule. In the approximation to the charging work (eq 5), the potential over the entire element is assumed to be the same as the potential at the node. This method systematically overestimates the repulsion between the proteins because the approximation is poorest for the elements that make the largest contribution to the charging work (those closest to the other sphere). Previous work has shown that the calculations converge toward the true solution, with an error that scales as $1/N$,²⁶ so increasing the number of elements would reduce the calculated repulsion. Second, including additional charge states would reduce the upper bound on the charging work calculated from eq 12, although this effect may be small. Preliminary work involving the 64 most likely charge states gives only a small change from the results presented here.

Third, Lenhoff has shown that the van der Waals attraction makes its greatest contribution to B_2 at separations on the order of 1 Å when the molecules can orient to present geometrically complementary surfaces.^{7,25} In these orientations, significant portions of the two molecules approach closely and produce a strong attraction that dominates the electrostatic repulsion. Because the current calculations do not preserve the detailed geometry of the molecules, this contribution to B_2 is neglected, and the estimated value of A_{eff} is too large.

Each source of variability in the protein’s charge distribution broadens the distribution of interaction energy about the mean and increases the number of low-energy charge configurations and molecular orientations. Consequently, the average electrostatic repulsion between particles is decreased, and the A_{eff} needed to match experiment is reduced. Including both types of charge distribution effects reduces the apparent ionic strength dependence of A_{eff} and brings the calculated values in better agreement with theory.

Discussion

Variations in the charge distribution reduce the net repulsion between like proteins. While the results above are based on a model where the possible charged sites are fixed on the surface, the side chains on proteins are not so tightly constrained. A more detailed model of protein–protein electrostatics, then, could allow for the extra degrees of freedom associated with this mode of charge redistribution. In the current numerical model, the charge associated with each group is assigned to specific surface elements. The effect of side chain mobility could be estimated by discretizing the surface with higher resolution and then allowing the charge associated with each ionizable group to occupy any element within the side chain’s range of motion. Since such charge rearrangement should lead to lower-energy configurations that are favored by Boltzmann weighting, side chain mobility will reduce the net repulsion between molecules of the same protein.

When the protein solution contains a mixture of different proteins, some proteins may have charges of opposite sign. For a patchy fixed charge distribution, the molecules will once again tend toward favorable orientations, and the effective attraction between unlike molecules will be stronger than for uniform fixed charges. The effect of charge fluctuations, however, is to reduce

the attraction. An analysis similar to that of eqs 13–17 yields the following asymptotic interaction potentials (through terms linear in ϕ_i):

$$\frac{\Phi_{\text{elec}}}{kT} = \bar{Z}_1 \bar{Z}_2 \phi_1 + (\bar{Z}_1^2 + \bar{Z}_2^2) \phi_2 \text{ (fixed charge)} \quad (21)$$

$$\frac{\Phi_{\text{elec}}}{kT} = \langle Z_1 \rangle \langle Z_2 \rangle \phi_1 + (\langle Z_1^2 \rangle + \langle Z_2^2 \rangle) \phi_2 \text{ (fluctuating charge)} \quad (22)$$

The first term is attractive because the proteins have opposite charges while the second term is repulsive. Since $\langle Z \rangle$ is Boltzmann-weighted according to the self-energy and the self-energy is proportional to Z^2 , $\langle Z \rangle$ is always smaller in magnitude than \bar{Z} . The reduction in average self-energy lowers the repulsion between like-charged proteins and reduces the attraction between differently charged proteins. While the interaction potential could be made more attractive by increasing the magnitude of the charge on each molecule, the extra self-energy required to do so leads to an increase in the total system energy and is not thermodynamically favored.

All the results reported here are based on the linearized Poisson–Boltzmann equation, which is valid for small electrostatic potentials. At low ionic strength, local surface potentials on the protein may significantly exceed 100 mV when the protein–protein separation is small. If the Poisson–Boltzmann equation (PBE) is not linearized, the behavior of the system will be somewhat different. First, the full Poisson–Boltzmann equation predicts surface potentials that tend to saturate at about 100 mV.²² The self-energy of the proteins would then be smaller than calculated from the linearized equation,¹⁶ and the average charge on the protein will be closer to \bar{Z} . Larger values of $\langle Z \rangle$ imply smaller effects for charge patchiness and charge fluctuation. Second, if the surface potentials are close to saturation, the incremental charging work required to bring the molecules together from infinity (the interaction potential) will be relatively small, and the repulsion between the proteins will be much weaker than estimated in this work. Without performing the calculations, however, it is difficult to determine how much of the reduction to attribute to the PBE itself and how much to charge variability.

Summary

Charge variability in both time and space plays an important role in determining the interactions between proteins in solution. Charge fluctuation works to minimize the magnitude of the average charge on the molecules and, thus, reduces the net repulsion between molecules. This mechanism contributes at all protein–protein separations and is most significant when the molecule contains many ionizable groups with pK_a s close to the pH in solution. In contrast, charge heterogeneity (patchiness) reduces the repulsion at separations smaller than the Debye

length, when multipole interactions become significant. Charge heterogeneity is also pH-dependent because the average charge distribution varies with pH. For the conditions studied here, the repulsion at contact between two molecules with patchy charge distributions is about 35% less than that for the equivalent uniformly charged molecules.

When the different charge distribution models are used to compute the second virial coefficient of lysozyme, the calculations show that including charge heterogeneity and charge correlation greatly reduces the apparent ionic strength dependence of the effective Hamaker constant. Furthermore, as each form of heterogeneity is added to the model, the best-fit values of A_{eff} approach those estimated from Lifshitz theory.

References and Notes

- (1) Kirkwood, J. G.; Shumaker, J. B. *Proc. Nat. Acad. Sci. U.S.A.* **1952**, *38*, 863–871.
- (2) Stigter, D.; Hill, T. L. *J. Phys. Chem.* **1959**, *63*, 551–556.
- (3) Vilker, V. L.; Colton, C. K.; Smith, K. A. *J. Colloid Interface Sci.* **1981**, *79*, 548–566.
- (4) Haynes, C. A.; Tamura, K.; Körfer, H. R.; Blanch, H. W.; Prausnitz, J. M. *J. Phys. Chem.* **1992**, *96*, 905–912.
- (5) Muschol, M.; Rosenberger, F. *J. Chem. Phys.* **1995**, *103*, 10424–10432.
- (6) McClurg, R. B.; Zukoski, C. F. *J. Colloid Interface Sci.* **1998**, *208*, 529–542.
- (7) Velev, O. D.; Kaler, E. W.; Lenhoff, A. M. *Biophys. J.* **1998**, *75*, 2682–2697.
- (8) Phillies, G. D. J. *J. Chem. Phys.* **1974**, *60*, 2721–2731.
- (9) Gilson, M. K.; Sharp, K. A.; Honig, B. H. *J. Comput. Chem.* **1987**, *9*, 327–335.
- (10) Yoon, B. J.; Lenhoff, A. M. *J. Comput. Chem.* **1990**, *11*, 1080–1086.
- (11) Grant, M. L.; Saville, D. A. *J. Phys. Chem.* **1994**, *98*, 10358–10367.
- (12) Glendinning, A. B.; Russel, W. B. *J. Colloid Interface Sci.* **1983**, *93*, 95–104.
- (13) Krozal, J. W.; Saville, D. A. *J. Colloid Interface Sci.* **1992**, *150*, 365–373.
- (14) Hill, T. L. *An Introduction to Statistical Thermodynamics*; Dover: Mineola, NY, 1986.
- (15) McQuarrie, D. A. *Statistical Mechanics*; Harper and Row: New York, 1976.
- (16) Sharp, K. A.; Honig, B. *J. Phys. Chem.* **1990**, *94*, 7684–7692.
- (17) Brebbia, C. A.; Telles, J. C. F.; Wrobel, L. C. *Boundary Element Techniques*; Springer-Verlag: Berlin, 1984.
- (18) Stryer, L. *Biochemistry*; W. H. Freeman and Company: New York, 1981.
- (19) Israelachvili, J. N. *Intermolecular and Surface Forces*, 2nd ed.; Academic Press: San Diego, 1992.
- (20) George, A.; Wilson, W. W. *Acta Crystallogr.* **1994**, *D50*, 361–365.
- (21) Verwey, E. J. W.; Overbeek, J. T. G. *Theory of the Stability of Lyophobic Colloids*; Elsevier: New York, 1948.
- (22) Russel, W. B.; Saville, D. A.; Schowalter, W. R. *Colloidal Dispersions*; Cambridge University Press: Cambridge, 1989.
- (23) Hunter, R. J. *Foundations of Colloid Science*; Clarendon Press: Oxford, 1987; Vol. 1.
- (24) Hiemenz, P. C.; Rajagopalan, R. *Principles of Colloid and Surface Chemistry*, 3rd ed.; Marcel Dekker: New York, 1997.
- (25) Roth, C. M.; Neal, B. L.; Lenhoff, A. M. *Biophys. J.* **1996**, *70*, 977–987.
- (26) Grant, M. L.; Saville, D. A. *J. Colloid Interface Sci.* **1995**, *171*, 35–45.